Journal of Membrane Science 547 (2018) 11–18

Contents lists available at ScienceDirect

Journal of Membrane Science

journal homepage: www.elsevier.com/locate/memsci

$Ce_{0.85}Sm_{0.15}O_2$-$Sm_{0.6}Sr_{0.4}Al_{0.3}Fe_{0.7}O_3$ composite for the preparation of dense ceramic-carbonate membranes for CO_2 separation

O. Ovalle-Encinia[a], H. Pfeiffer[a], J. Ortiz-Landeros[b,*]

[a] Laboratorio de Fisicoquímica y Reactividad de Superficies (LaFReS), Instituto de Investigaciones en Materiales, Universidad Nacional Autónoma de México, Circuito exterior s/n, Cd Universitaria, Del. Coyoacán, CP 04510 Ciudad de México, Mexico

[b] Departamento de Ingeniería en Metalurgia y Materiales, Escuela Superior de Ingeniería Química e Industrias Extractivas, IPN, UPALM, Av. Instituto Politécnico Nacional s/n, CP 07738 Ciudad de México, Mexico

ARTICLE INFO

Keywords:
Ceramic-carbonate
Dual-phase membrane
CO_2 permeation
Perovskite
Fluorite

ABSTRACT

In the last years, it has been proposed the use of ceramic-carbonate dense membranes to separate CO_2, selectively from combustion gas, at high temperatures. The mechanism of CO_2 separation of these membranes involves the transport of O^{2-} ions through the ceramic phase of the membrane. Thus, the present study examines the $Ce_{0.85}Sm_{0.15}O_2$-$Sm_{0.6}Sr_{0.4}Al_{0.3}Fe_{0.7}O_3$ composite to prepare such a ceramic-carbonate membrane, as this composite has been previously reported as an excellent oxygen conductor. Firstly, the composite was prepared by two different synthesis pathways, both based on the EDTA-citrate complexing method. Subsequently, disk shape membrane supports were produced by pressing selected powder samples and they were evaluated in terms of their thermal and chemical stability. Furthermore, ceramic-carbonate membranes were prepared via direct infiltration with molten carbonates and evaluated at high temperatures for the CO_2 separation. Results suggest the possible application of this composite for the fabrication of stable dense membranes performing selective CO_2 separation at high temperatures (700–900 °C).

1. Introduction

The industrial activity has increased in the last decades which is directly related with the raise in the fossil fuels consumption and the consequent overproduction of CO_2 emitted to the atmosphere [1]. Since CO_2 is the major greenhouse gas producing the global climate change issue [2,3], many researchers are focused on the development of new materials and technologies for the separation, capture or storage of the CO_2 content in the flue gas emitted from power plants [4] and other industrial processes [5]. Several emerging CO_2 capture technologies have been studied to be applied to pre- and post-combustion processes [6,7]. Moreover, separation technologies such as the so called dense dual-phase membranes have been proposed as an affordable means to reduce hazardous CO_2 emissions. In the later, as the combustion gas is released at high temperatures, it would be convenient to separate CO_2 in the same temperature range [8]. Additionally, the idea of a separation process performed by a membrane at elevated temperatures means that the CO_2 permeated could be used as raw material or carbon source to make reactions such as the dry reforming of methane, producing syngas [9,10].

The dense dual-phase membranes are made of a porous solid support infiltrated with molten carbonates, wherein the solid support is a metal or an oxygen ionic conductor ceramic phase. The first report of this kind of membranes was published by Lin and coworkers [11]. After that work, several ceramic-carbonate dual-phase systems have been studied to separate CO_2 at high temperatures. Among them, solid oxide phases such as yttrium-doped zirconia, gadolinium-doped ceria and samarium-doped ceria have presented favorable results from the point of view of membrane stability and relatively high CO_2 permeation flux [12,13].

CO_2 permeation, in ceramic-carbonate membranes, is due to the reaction of the oxygen ions coming from the ceramic oxide with the CO_2 feed gas in the upstream side of the membrane. This reaction produces carbonate ions (CO_3^{2-}, see reaction 1), which will pass through the molten carbonates because of a CO_2 partial pressure gradient. Finally, in the downstream side of the membrane the reversible reaction takes place. Therefore, the oxygen ions return to the ceramic phase via the vacancies diffusion process, while CO_2 is released as the permeated gas.

$$CO_2 + O_0^X \leftrightarrow CO_3^{2-} + V_{\ddot{O}} \quad (1)$$

Some perovskites have been analyzed and used to prepare dense ceramic-carbonate membranes, i.e., $La_{0.6}Sr_{0.4}Co_{0.8}Fe_{0.2}O_{3-\delta}$ [14,15]

* Corresponding author.
E-mail address: jortizla@ipn.mx (J. Ortiz-Landeros).

http://dx.doi.org/10.1016/j.memsci.2017.10.021
Received 16 February 2017; Received in revised form 4 October 2017; Accepted 9 October 2017
Available online 10 October 2017
0376-7388/

and $La_{0.85}Ce_{0.15}Ga_{0.3}Fe_{0.65}Al_{0.05}O_{3-\delta}$ [16]. These perovskites are well known mixed ionic-electronic conductors and it has been concluded that in these cases, the CO_2 permeation process can take place with or without the presence of O_2 in the feed gas [17]. Like the case of membranes made of ionic conductors as the solid phase, the surface reaction without O_2 in the feed gas is described by reaction 1. On the other hand, if a chemical gradient of O_2 is present, reaction 2 must be considered.

$$\frac{1}{2}O_2 + V_O^{\cdot\cdot} \leftrightarrow O_0^X + 2h^{\bullet} \quad (2)$$

Ceramic-carbonate membranes prepared with perovskites have shown high CO_2/N_2 selectivity values and relatively high permeation flux. However, it is important to mention that these materials have shown certain stability issues due to the perovskite decomposition under low oxygen partial pressures, as well as under CO_2 rich environments [14].

Recently, a $Ce_{0.85}Sm_{0.15}O_2$–$Sm_{0.6}Sr_{0.4}Al_{0.3}Fe_{0.7}O_3$ (SDC-SSAF, 75–25 wt%) based composite membrane was analyzed for oxygen permeation [18]. It was observed a high permeation flux from 0.35 to 0.70 mL cm^{-2} min^{-1} at 800 to 950 °C, respectively. Additionally, the study showed the membrane stability under a CO_2 sweeping. Therefore, the fabricated membrane was proposed for the oxy-fuel process. Then, since the mechanism of CO_2 separation, in the ceramic-carbonate membranes involves the transport of O^{2-} ions through the ceramic phase of the membrane; this study examines the SDC-SSAF composite to prepare such a ceramic-carbonate membrane as it has been reported as an excellent oxygen conductor and a chemically stable material under CO_2 saturated atmospheres.

2. Experimental procedure

2.1. Synthesis of $Ce_{0.85}Sm_{0.15}O_2$-$Sm_{0.6}Sr_{0.4}Al_{0.3}Fe_{0.7}O_3$ (SDC-SSAF) composite powders

SDC-SSAF powders were synthesized by two methods, as it has been previously proposed by Zhu et. al. [19]. The first synthesis method consisted in preparing the composite powders by a so-called one-step approach, via the EDTA-citrate complexing method [19]. Initially, two solutions were prepared; one of the fluorite phase precursor with the corresponding stoichiometric amounts of metal nitrates (Ce $(NO_3)_3{\cdot}6H_2O$, 99.0% Sigma-Aldrich and $Sm(NO_3)_3{\cdot}6H_2O$, 99.9% Sigma-Aldrich) and another solution of the perovskite phase precursor (Sm $(NO_3)_3{\cdot}6H_2O$, 99.9% Sigma-Aldrich, $Sr(NO_3)_2$ 99.0% Meyer, Al $(NO_3)_3{\cdot}9H_2O$, 98% Sigma-Aldrich and $Fe(NO_3)_3{\cdot}9H_2O$, 98% Meyer). Then, both solutions were dissolved in deionized water, followed by addition of anhydrous citric acid (99.98% Sigma-Aldrich) and EDTA (98.5% Sigma-Aldrich), which was previously dissolved in ammonium hydroxide (28.0–30.0%, BAKER ANALYZED® A.C.S. Reagent). An equimolar ratio between citrate and EDTA were added respect to the total metal ions. Then, pH value was adjusted to 7–8 by adding ammonium hydroxide in both solutions. Finally, both solutions were mixed together to obtain a 75–25 wt% ratio of the fluorite (SDC) and perovskite (SSAF) constituents. This solution was subsequently heated up to 90 °C, while stirring. After water evaporation, a black gel was produced. Then the gel was combusted at about 300 °C to remove the organic matter. The resultant yellow powder was calcined at 650 °C for 10 h and then at 900 °C for 10 h. On the other hand, the second method consisted in synthesizing each pristine phase (SDC and SSAF) separately, using the same combined citric acid-EDTA process [19] as it was described above. Then, the obtained powders were mixed together during 10 min using a SpectroMill II ball mill equipment to finally obtain a mixture of 75 wt% SDC and 25 wt% of SSAF phases.

2.2. Preparation of (SDC-SSAF)-carbonate membranes

Firstly, to fabricate the porous supports, approximately 4 g of SDC-SSAF composite powders with 1 wt% of polyvinyl alcohol (PVA) as binder was placed into a 26 mm diameter stainless steel die and pressed up to 6 t for 6 min in a hydraulic press. The pressed disks were then sintered in air for 40 h at 900, 1000 or 1100 °C at 1 °C/min to obtain porous supports. No pore former was added for the fabrication of these supports. After the sintering process, dense dual-phase membranes made of composite (SDC-SSAF)-carbonate were prepared by direct infiltration of porous supports at 600 °C, using an eutectic molten carbonate mixture composed of $Li_2CO_3/Na_2CO_3/K_2CO_3$ with a molar ratio of 42.5/32.5/25.0. After the membrane infiltration and cooled down processes, the excess of carbonates remaining on the membrane surface was removed by polishing the membrane in both sides.

2.3. Material characterization

A diffractometer (Bruker, D8 Advance) with a Cu-Kα (1.54059 Å) radiation source operating at 35 kV and 30 mA was used to identify the SDC fluorite and SSAF perovskite crystalline phases after the synthesis and sintering processes, as well as to examine the structural stability of the supports after their exposure to a rich CO_2 environment. Samples were measured in the 2-theta range of 20–120° with a step size of 0.02°. The phases were identified using the Joint Committee Powder Diffraction Standards (JCPDS) data base and crystalline structures were refined with the Rietveld method by using the BGMN program [20] and the graphical interface Profex [21]. Peak profiles were modeled with a Lorentzian function to determine the crystal size anisotropy using the Debye-Scherrer formula [22] and spherical harmonics as base functions to model the reflection width parameters as a function of the Miller indices. Additionally, the membranes morphology was analyzed using a scanning electron microscopy (SEM). The SEM analysis was performed on a JEOL JMS-7600F. The controlled atmosphere experiments were performed to analyze the thermal and chemical stability of the SDC-SSAF composite powders. These experiments consisted in placing the SDC-SSAF disk inside to a tubular furnace at 900 °C for 20 h in a rich CO_2 environment; wherein the furnace chamber was feed with a 100 vol% CO_2 gas (Praxair, grade 3.0) using a 60 mL min^{-1} flow rate; after the test, the products were analyzed by XRD. Additionally, thermogravimetric analyses (TGA) were performed as a first assessment to elucidate the thermal stability of the ceramic-carbonate composite. The dual-phase membrane sample was analyzed using a Q500HR equipment from TA Instruments. Sample was heat treated with a heating rate of 5 °C/min from room temperature to 950 °C. These analyses were carried out under CO_2 atmosphere, using a gas flow of 60 mLmin^{-1}.

2.4. High temperature CO_2 permeation measurements

High temperature CO_2 permeation measurements were conducted between 700 and 900 °C, using the experimental set-up illustrated in Fig. 1. The (SDC-SSAF)-carbonate membranes were sealed to an inner alumina tube by creating a ceramic sealant paste. The sealant was composed by SDC-SSAF powder mixture sintered at 1000 °C (40 wt%), Pyrex glass powder (50 wt%) and sodium aluminum oxide (Al_2O_3 Na_2O; 10 wt%), mixed with deionized water. The system was completely sealed inside a 50 mm outer diameter dense alumina tube and heated at a rate of 3 °C/min from room temperature to 900 °C allowing the glass phase to melt and form a tight sealing. The following feed gas mixtures were used for the CO_2 permeation experiments; CO_2/He (15/15 mL min^{-1}) and CO_2/He/O_2 (15/15/6 mL min^{-1}) with N_2 balanced to 100 mL min^{-1}. In all cases, N_2 was used as sweeping gas in the downstream side of the membrane test array. The permeate gas was analyzed with a GC-2014 gas chromatograph (Shimadzu) equipped with a Carboxen-1000 column.

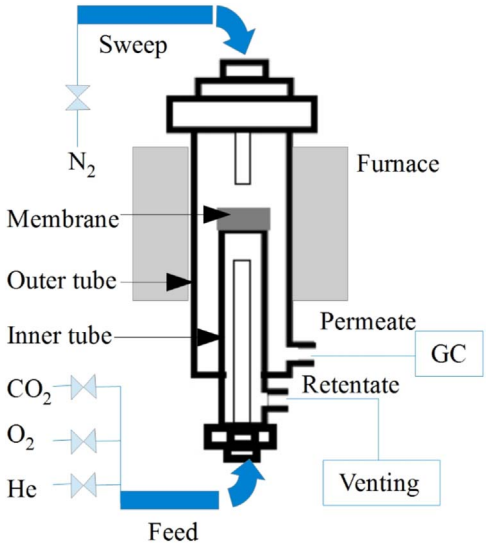

Fig. 1. Representative scheme of the home-made permeation set-up.

3. Results and discussion

3.1. Crystal structure and microstructure of the composite powders

After the synthesis process of the single pristine ceramic powders and the composite, X-ray diffraction pattern was obtained for each sample. Fig. 2 shows the XRD patterns of the pristine SDC and SSAF powders as well as the resulting composite, after the ball milling process. The XRD pattern of the SDC sample only showed diffraction peaks indexing with the PDF 43-1002 file, corresponding to the cerium oxide phase with a fluorite crystal structure. Also, the SSAF sample fitted to the perovskite phase corresponding to PDF 28-1227 file. None of these two samples presented the formation of any secondary phases, at least at the XRD detection limit. The mixed sample shows the reflections of both phases, (SDC and SSAF), as it could be expected. Nevertheless, it is important to mention that both phases remained stable after the ball milling process.

Fig. 3 shows the XRD patterns of the composite powders synthesized by one step method and obtained after the calcination at 650 and 900 °C for 10 h. In the first case, XRD profile shows broad reflections that are features of a low crystallinity. Then, after calcination at 650 °C it is evident the peak reflections of the fluorite phase but the perovskite

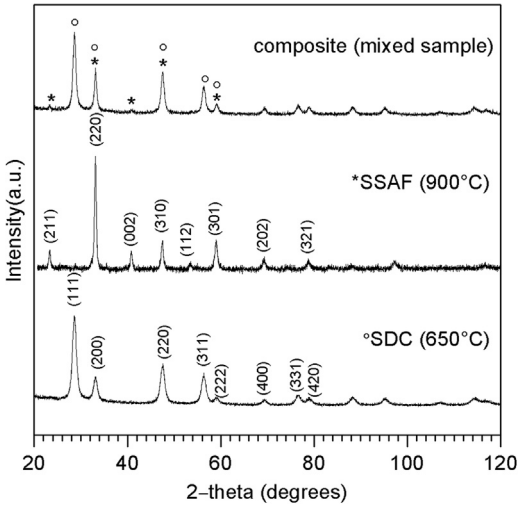

Fig. 2. XRD patterns of SDC, SSAF and composite samples. (°) SDC fluorite diffraction peaks (PDF43-1002 file) and (*) SSAF perovskite diffraction peaks (PDF 28-1227 file).

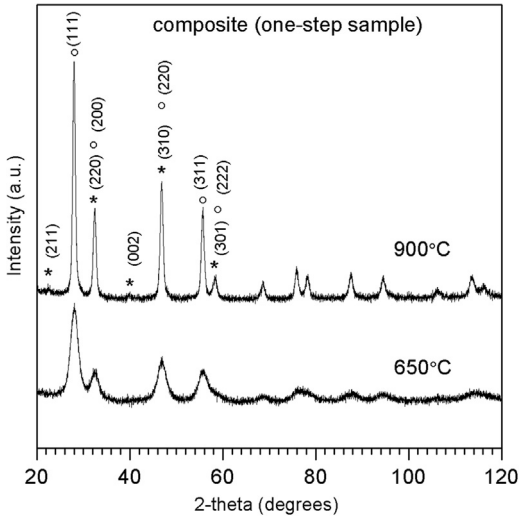

Fig. 3. XRD patterns of the one-step samples after their synthesis at two different temperatures of calcination. (*) perovskite diffraction peaks (PDF 28-1227 file) and (°) fluorite diffraction peaks (PDF 43-1002 file).

phase reflections are not observed, suggesting that the perovskite phase may have not been completely crystallized at 650 °C. However, the sample heated at 900 °C shows the presence of both, the fluorite and perovskite phases. Although most of the perovskite reflection peaks overlaps with the fluorite reflections, the (211) and (002) perovskite reflections are clearly identified. Moreover (200) fluorite reflection may be enhanced due to the overlapping of the most intense reflection (220) of the perovskite. In both samples, no impurities were observed, therefore, the SDC and SSAF phases present in the composite shown chemical compatibility.

Depending on the synthesis pathway there are certain differences between the mixed and the one step method samples. In this sense a structural analysis of the samples was carried out by Rietveld refinement. The cubic fluorite structure SDC was modeled the FM3M (225) space group, while the SSAF cubic structure was analyzed with the PM-3M (221) space group. Tables 1 and 2 shows the initial crystallographic data for all the crystalline phases and their Rietveld refinement results, respectively. The results in Table 2 does not show remarkable differences between the unit cell parameters of SDC in the three different samples. In other words, the Sm^{3+} doping was not affected by the synthesis pathway in fluorite phase. On the other hand, both the SSAF cell parameter and cell volume exhibited slight differences between the different composite samples in comparison with the single sample. Despite more cations are involve in the SSAF phase case, and the evolution of this structure should be more complex; the observed changes can be explained considering that the average cell parameter of the unit cells was affected by the atomic substitution of the species in the

Table 1
Initial crystallographic information used for the Rietveld refinement method.

	Space group	Cell parameters a(Å)	Atomic positions			
			Atom (site Wyckoff)/ occ	x (fracc.)	y (fracc.)	z (fracc.)
SDC	*FM-3M* (225)	5.4110	O (a) 1	1/2	1/2	1/2
			Ce/Sm (c) 0.85/0.15	0	0	0
SSAF	*PM-3M* (221)	3.856	Sr/Sm (b) 0.6/0.4	1/2	1/2	1/2
			Fe/Al (a) 0.3/0.7	0	0	0
			O (d) 1	0	0	1/2

Table 2
Rietveld refinement results of the one-step, mixed and single samples after synthesis.

		One-step	Mixed	Single SDC (900 °C)	Single SSAF (900 °C)
Rwp (%)		5.64	5.69	7.49	4.2
χ^2		1.10372	1.1201	1.2442	1.28049
SDC	a (Å)	5.4371(5)	5.4310(6)	5.4311(1)	–
	Vol. cell (Å^3)	160.73(4)	160.19(5)	160.17(1)	–
	wt%	78(1)	73(2)	100	–
SSAF	a (Å)	3.873(1)	3.8404(7)	–	3.8450(4)
	Vol. cell (Å^3)	58.10(5)	56.64(3)	–	56.84(2)
	wt%	22(1)	27(2)	–	100

perovskite sites A and B. In the case of the mixed sample the volumetric change was negligible, but in the one-step sample the Fe^{3+} ($r_{Fe^{3+}} = 0.64$Å) substitutes to Al^{3+} ($r_{Al^{3+}} = 0.5$Å) and Sm^{3+} ($r_{Sm^{3+}} = 0.96$Å) replaces to Sr^{2+} ($r_{Sr^{2+}} = 1.13$Å) producing a total average dimensional change of 0.78% (relatively to the unit cell of the single sample), which is in agreement with the volume change calculated by Rietveld refinement. Furthermore, regarding the theoretical composition of the composite, the SDC and SSAF weight percent showed a deviation from the nominal 75–25 wt%, which is specially observed in the one-step composite. In the case of the one-step sample, the high error detection of SSAF could be attributed to the formation of small crystallites and its homogeneous distribution into the SDC majority phase, as result of the nucleation and growth processes. Therefore, the detection by XRD of those small SSAF structures is hindered by the fluorite phase.

The scanning electron microscopy images (Fig. 4) show the effect of the preparation method of the single and composite samples. These images evince the obtaining of different morphologies, particle size distributions and the presence of aggregates. Fig. 4a shows pristine SDC powders, forming plate particles of around ~ 6 μm. The Fig. 4b shows the SSAF powders with an irregular shape, having a particle size of ~ 2 μm. The mixed composite sample shows a slightly more homogeneous particle shape and narrow particle size distribution (Fig. 4c). These features were attributed mainly due to the ball mill effect. On the contrary, Fig. 4d shows the one step composite sample, which exhibits a polyhedral heterogeneous distribution of particles with an average particle size smaller than 2 μm.

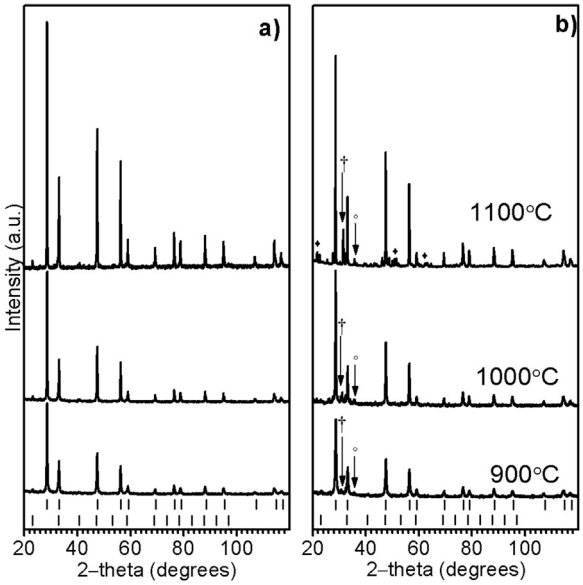

Fig. 5. XRD patterns of the a) one-step and b) mix disk samples at different sintering temperatures. Lower vertical marks (*) perovskite diffraction peaks (PDF 28–1227 file) and upper vertical marks (°) fluorite diffraction peaks (PDF43-1002 file). Secondary phases corresponding to (†) SmO, (°) Fe_2O_3 and (◆) unidentified.

The thermal and chemical stability tests were performed for the mixed and one step composite disk samples. This analysis was performed in order to determine the stability of the SDC-SSAF composites under a CO_2 rich atmosphere and elevated temperatures like the expected operation conditions for a dual-phase membrane. Fig. 5 shows the XRD patterns after the thermal treatment at different temperatures of both composite samples. Fig. 5a shows the XRD patterns of the one-step sample heated between 900 and 1100 °C. These XRD patterns show a high thermal stability of the composite, as it was not observed the presence of any secondary phase. Therefore, this composite is stable and its components are compatible each other at high temperatures. On the contrary, Fig. 5b shows the corresponding XRD patterns of the mixed sample, where it was evidenced the formation of secondary phases; samarium oxide (SmO), iron oxide (Fe_2O_3) and other

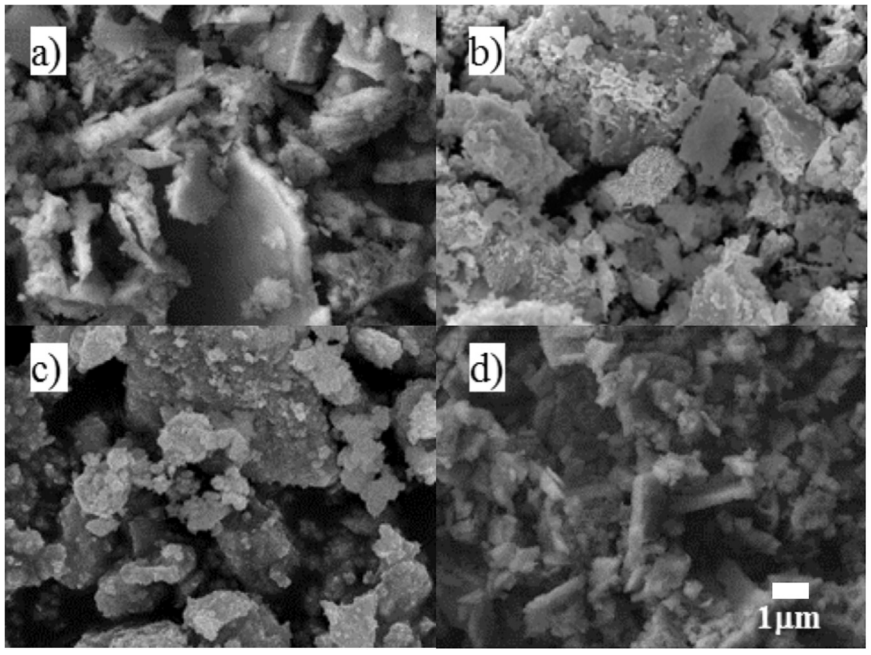

Fig. 4. SEM images of the ceramic powders: pristine phases a) SDC and b) SSAF, c) mixed sample and d) one-step sample.

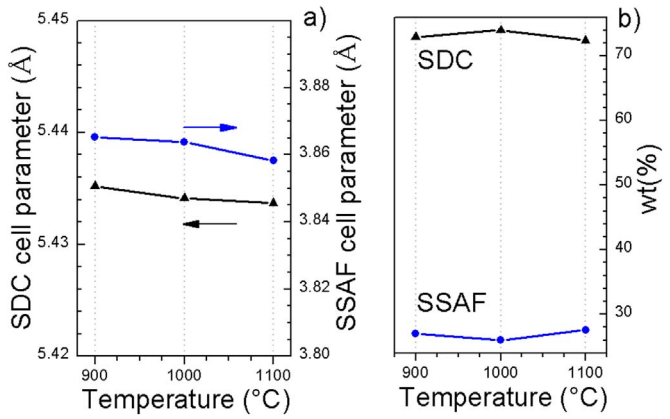

Fig. 6. Rietveld refinement results of the one-step sample sintered at different temperatures.

unidentified peaks. Therefore, the mixed composite seems to be less thermally stable than the one step sample.

The aforesaid XRD patterns were analyzed by the Rietveld method, thus the samples structural parameters were examined. The cell parameters of SDC and SSAF phases in the one-step sample did not presented remarkable differences among the samples heat treated at different temperatures (Fig. 6a). Besides, the total weight percent of the phases in this composite showed no significant variation as a function of the temperature (Fig. 6b). On the other hand, while the cell parameters of the SDC in the mixed composite did not show noticeable changes (change lower than 0.17%) by effect of the temperature, it can be seen how the SSAF cell parameter changed 0.70% (Fig. 7a), which is in agreement with the total average dimensional change of 0.78% mentioned previously. Also, the total weight percent of this phase, in the composite, changed remarkably as the calcination temperature increased (Fig. 7b). For example, the total constituents were calculated as 89.6(8), 1.5(1), 2.8(2) and 6.1(9) wt% of SDC, SSAF, SmO and FeO respectively (the last two measurements are not shown in the graph), when the sample was heat treated at 1000 °C. Moreover, at 1100 °C it was observed that the amount of secondary phases increased. In fact, the SmO and FeO reache 5.4(2) and 8(1) wt%, respectively. Based on the above, it was evidenced that the perovskite in the mixed composite is prone to thermally decomposed mainly into the aforementioned oxides, and the rest of the cations might be forming unidentified phases or become dopants in the other oxides. As the composite mixed sample was prepared by ball milling using a high energy ball mill apparatus; the observed instability of the sample was attributed to the sample mechanical activation during the milling process. Actually, this kind of milling process is able to promote not only mixing or particle size reduction, but chemical reactions.

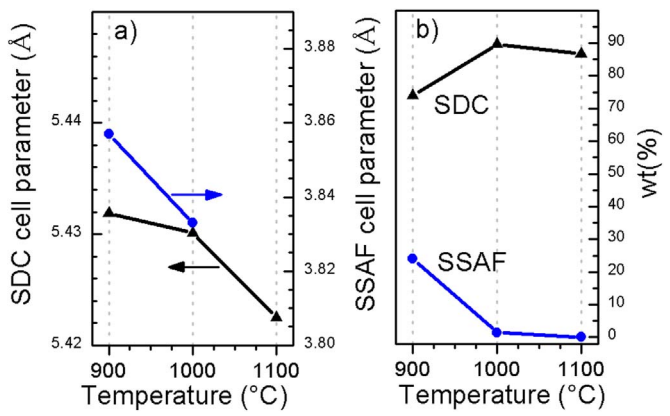

Fig. 7. Rietveld refinement results of the mixed sample sintered at different temperatures.

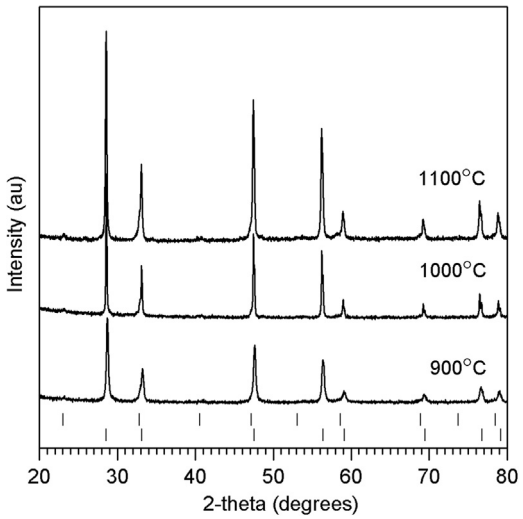

Fig. 8. XRD patterns of one-step disk samples sintered at different temperatures after the CO_2 stability tests. Lower vertical marks (*) perovskite diffraction peaks (PDF 28-1227 file) and upper vertical marks (°) fluorite diffraction peaks (PDF 43-1002 file).

Based in all the previous results, the mixed sample was discarded due to its lower thermal stability in comparison to the one-step sample and only the later one was evaluated for CO_2 stability. For this test, sample was exposure to a saturated CO_2 atmosphere (100%) between 900 and 1100 °C during 20 h. Fig. 8 shows the XRD patterns of the samples after such a test, where the results only showed the presence of SDC and SSAF crystalline phases, evidencing their thermal and chemical stability.

3.2. Dual-phase membrane preparation and stability test

As it was already mentioned at the experimental section, membrane supports were prepared by pressing and sintering the composite powders. Fig. 9a shows the scanning electron microscopy image of a composite disk support sintered at 1100 °C. The image obtained with backscattered electrons shows the support porosity, which is about 48.6 vol% of the solid phase. The open porosity value was estimated following the immersion Archimedean method [23]. Then, the pellet was impregnated with molten carbonates to form the dense dual-phase membrane made of composite-molten carbonates, (Fig. 9b). Dark zones correspond to carbonates, while the grey zones are the composite particles. The resulted ceramic-carbonate dense membrane did not show cracks, and a homogeneous distribution of the components wherein the carbonate fills up the initial open porosity.

In order to evaluate the stability between the SDC-SSAF ceramic and the molten carbonates at high temperatures, the prepared dense membrane was analyzed by thermogravimetry under a saturated CO_2 atmosphere (100%). Fig. 10a shows the TG curve, which reveals two slight mass variations. An initial mass increment (0.2 wt%) take place between 320 and 500 °C and it can be attributed to the carbonates fusion and equilibrium processes, as the sorption can be performed with the ternary carbonate mixture due to its lower melting point (397 °C). Then, a second process was observed, a decrement of 0.7 wt%, at temperatures higher than 700 °C and it can be attributed to both, the partial decarbonation process and the potential release of oxygen from the ceramic phase under the low oxygen partial pressure. Although, the membrane presents such a small total loss of mass (~ 0.5 wt%), the XRD pattern of the sample after the stability test shows structural stability of the material, as no other crystal phases were detected (Fig. 10b). Once again, the diffraction peaks were only indexed with SDC and SSAF phases and there were not diffraction peaks corresponding to the carbonates, as they were composed of lighter elements and exhibits low diffraction intensities. Moreover, there is not any

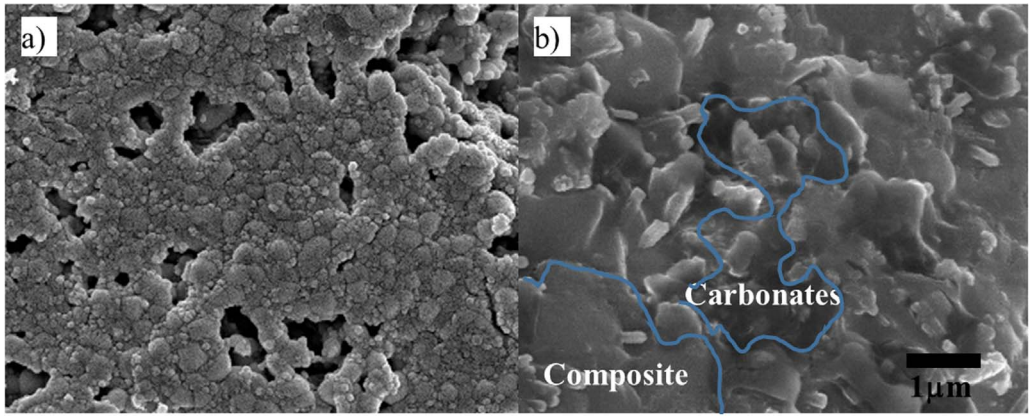

Fig. 9. Backscattered electron images of one-step disk sample sintered at 1100 °C: a) surface view of the support before impregnation and b) cross sectional microstructure of the dual-phase membrane.

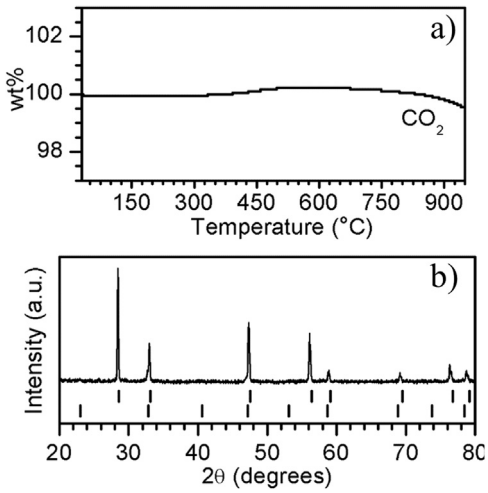

Fig. 10. a) Dynamic thermogravimetric analysis in CO_2 atmosphere and b) XRD pattern after the thermogravimetric test of the dense ceramic-carbonate membrane.

evidences of reaction between carbonates and SDC or SSAF constituents of the ceramic phase.

3.3. CO_2 permeation test

Fig. 11 shows the He and CO_2 permeation at high temperatures (700–900 °C), where a CO_2/He/N_2 gas mixture was feed (15/15/70 vol % mixture). As it can be seen, the helium permeability never exceeded 21×10^{-9} mol m^{-2} s^{-1} Pa^{-1}. Moreover, helium leak tends to decreases to a minimum value of 3×10^{-9} mol m^{-2} s^{-1} Pa^{-1} once the permeation temperature reaches 900 °C. This result is in agreement with the fact that glass-ceramic seals, seats and reaches gas tight at high temperature. It is important to have in mind that helium permeability could be only caused by leaking through microstructural defects in the membrane such as; unfilled pores, small cracks and remained porosity in the seal. Therefore, to correct the CO_2 permeation flux for any contribution due to leaking (considering Knudsen flow), 0.3 times of the helium permeability is subtracted from that of CO_2 (Eq. (3)). As expected, the CO_2 permeation flux tends to increase as the temperature increases reaching a maximum value of 1.7×10^{-7} mol m^{-2} s^{-1} Pa^{-1} at 900 °C. It is an important result considering the low partial pressure of CO_2 used in the feed side ($P_{CO2} = 0.15$). The CO_2/He selectivity was calculated and it was equal to 40.

$$P_{corrected} = P_{CO_2} - 0.3P_{He} \quad (3)$$

The results of the CO_2 permeation tests with different feed gas mixtures are shown in Fig. 12. As it was mentioned, the first test was performed using a feed gas mixture composed by CO_2/He/N_2 and the second test with a CO_2/He/O_2/N_2 gas mixture; in both cases N_2 was used as a carrier and sweeping gas. As it can be seen, temperature enhances the CO_2 permeation through the membrane as the transport of the involved species (O^{2-}) through the dense bulk membrane is a thermally activated process. Moreover, the oxygen addition in the feed

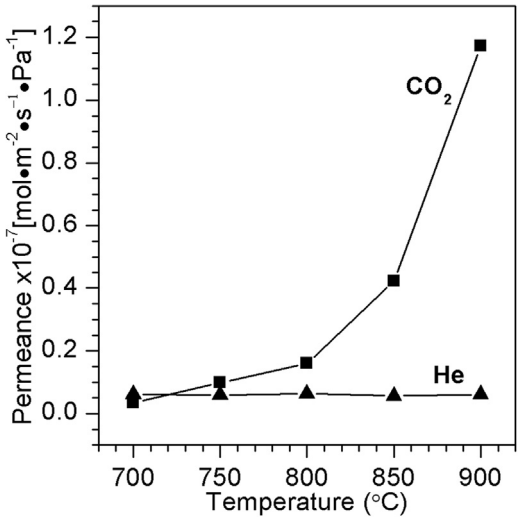

Fig. 11. High temperature CO_2 permeation of the dense membrane SDC-SSAF-molten carbonate. The feed gas mix used was CO_2/He/N_2 (15/15/70 vol%).

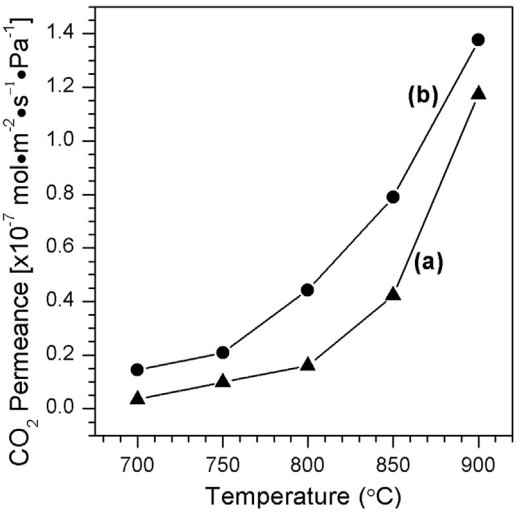

Fig. 12. High temperature CO_2 permeation of the dense SDC-SSAF-carbonate membrane using different feed gas mixtures; a) CO_2/He/N_2 and b) CO_2/He/O_2/N_2.

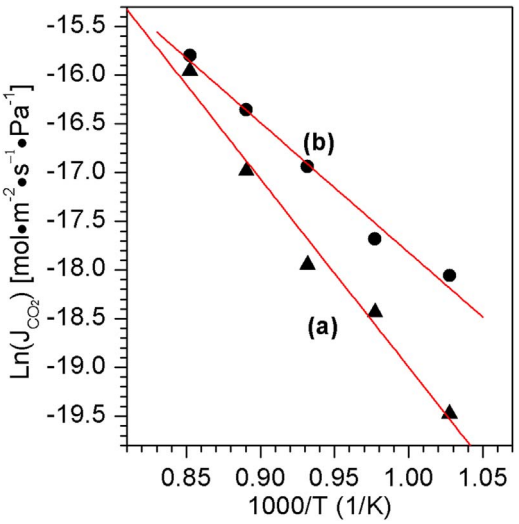

Fig. 13. Arrhenius plots of the CO_2 permeation test at high temperatures, using different gas mixtures; a) $CO_2/He/N_2$ and b) $CO_2/He/O_2/N_2$.

improves the CO_2 permeation process in the whole range of temperatures studied. Thus, an electrochemical reaction may occur where the oxygen species allow the production of CO_3^{2-}. In this case, it is expected that not only the oxygen ionic conductivity properties of the solid phase are involved, but the electronic conductivity of the ceramic phase must also contribute to the permeation process (reaction (4)). Therefore, the mechanism proposed for the mixed-conducting ceramic oxide [24] can be used to explain the observed increment in the permeation with the presence of oxygen.

$$CO_2 + \frac{1}{2}O_2 + 2e^- \leftrightarrow CO_3^{2-} \quad (4)$$

Fig. 13 shows the Arrhenius plot for CO_2 permeation versus temperature using different feed gas mixtures. The apparent activation energies for permeation process are 160.7 and 110.6 kJ mol^{-1} for the $CO_2/He/N_2$ and $CO_2/He/O_2/N_2$ feed gas mixtures respectively. These results show that oxygen addition decreases the activation energy for the CO_2 permeation.

The observed total O_2 permeation ($P^T_{O_2}$), is shown in the Fig. 14. Oxygen permeation flux exhibits the typical temperature dependence wherein the flux increases from 1.13 to about 1.65 × 10^{-7} mol m^{-2} s^{-1} Pa^{-1} from 700 to 900 °C, respectively. In theory,

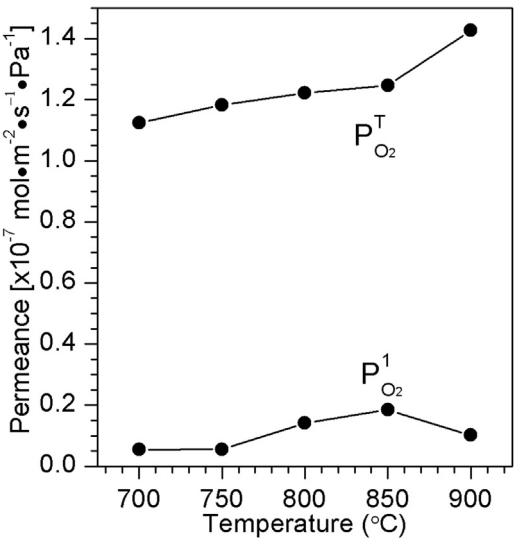

Fig. 14. Total O_2 permeation ($P^T_{O_2}$) and O_2 permeated by forming CO_3^{2-} ($P^1_{O_2}$).

Table 3
CO_2 Permeability values observed for different dual-phase membranes made of single perovskite and fluorite phases.

Composition	Temperature (°C)	Permeability mol m^{-1} s^{-1} Pa^{-1}	Ref.
$Ce_{0.8}Sm_{0.2}O_2$	700	3.53 × 10^{-11}	[25]
$Y_{0.16}Zr_{0.84}O_2$	650	2.4 × 10^{-13}	[12]
$Bi_{1.5}Y_{0.3}Sm_{0.2}O_3$	650	5.5 × 10^{-13}	[26]
$La_{0.6}Sr_{0.4}Co_{0.8}Fe_{0.2}O_3$	700	3.0 × 10^{-12}	[15]
$La_{0.85}Ce_{0.1}Ga_{0.3}Fe_{0.65}Al_{0.05}O_3$	900	4.5 × 10^{-12}	[16]
SDC-SSAF	700	1.82 × 10^{-10}	This work

this total oxygen permeation also involves certain amount of O_2 permeated by forming CO_3^{2-} ($P^1_{O_2}$), as describe in reaction (4). Therefore, Eq. (5) was used to estimate the aforesaid contribution.

$$P^1_{O_2} = \frac{P''_{CO_2} - P'_{CO_2}}{2} \quad (5)$$

where P'_{CO_2} and P''_{CO_2} are the CO_2 permeation using $CO_2/He/N_2$ and $CO_2/He/O_2/N_2$ feed gas mixtures respectively. Besides, in this specific case, $P^1_{O_2}$ first slightly increases with the increase of temperature from 700 to 850 °C and it seems to decrease at temperatures higher than 900 °C. The observed behavior could be explain due to the decrease in electronic carrier concentration at elevated temperatures, which is in fact a phenomenon frequently observed in Fe-based mixed conducting perovskites showing metallic behavior at elevated temperatures [15]. Actually, the total conductivity data reported for the SDC-SSAF system [18] is in the agreement with the present result. Then, at this elevated temperature the ionic conduction prevails in both SDC and SSAF single phases of the composite.

Table 3 Shows the CO_2 permeability values of different dual-phase membranes made of single perovskite and fluorite phases. The permeability values observed for the SDC-SSAF based membrane studied here is presented for comparative purposes.

Finally, in order to elucidate the thermal and chemical stability of the studied system, the tested membrane was analyzed by XRD technique. Fig. 15 shows the XRD patterns of samples before and after the CO_2 permeation tests. The analysis of the sweep side of the membrane does not show the formation of secondary phases that suggest its stability. On the other hand, in feed side case, results show the formation of $Al_8K_8O_{16}$ COD (Crystallographic Open Database) number 96-210-

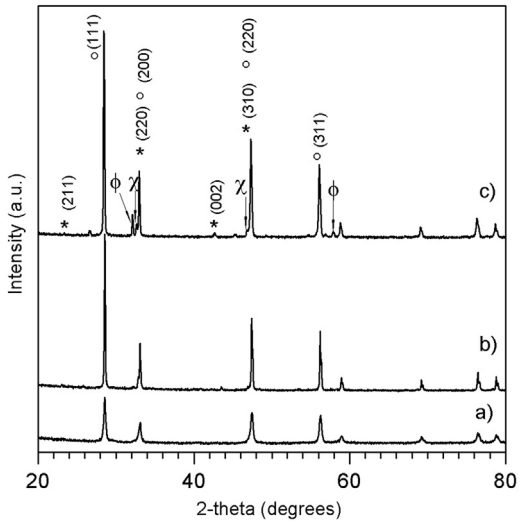

Fig. 15. XRD data of dense SDC-SSAF-carbonate membrane sintered at 1000 °C; a) before CO_2 permeation test, b) sweep side after CO_2 permeation test and c) feed side after CO_2 permeation test. φ and χ are the $Al_8K_8O_{16}$ and $Al_2K_2O_4$ formed phases.

5209 and $Al_2K_2O_4$ COD 96-210-5202. The formation of these secondary species was attributed to the use of the ceramic sealing. Actually, this kind of sealing is an experimental limitation to carry out long stability tests in membranes because of both, the contamination of the membrane and the presence of leaks after short times at elevated temperatures. Further research must be accomplished in order to elucidate the effect of longer operation times on the stability of this kind of membranes.

Based on all the above, the studied composite present good qualities for the preparation of thermally and chemically stable ceramic-molten carbonates dense membranes exhibiting high CO_2 permeation with or without the presence of oxygen in the feed gas mixture. In this case, the ceramic phase is made of a fluorite phase (ionic conductor) and a perovskite (ionic-electronic conductor) which can transport oxygen ions, while the CO_3^{2-} is permeated through the molten carbonates. Additionally, in this system, O_2 tends to increase the CO_2 permeation due to a faster anionic process produced into the composite by the contribution of the perovskite electronic properties, which does not obstruct the CO_2 permeation.

4. Conclusions

The $Ce_{0.85}Sm_{0.15}O_2$-$Sm_{0.6}Sr_{0.4}Al_{0.3}Fe_{0.7}O_3$ composite powders were synthesized by one-step and mixture method using the EDTA-citrate complexing method. Composite supports in a disc shape were prepared and sintered, but only the composite synthesized by one-step method presented thermal and chemical stability in air and CO_2. Moreover, using the composite prepared by the one-step method, dense membranes were successfully fabricated by direct infiltration of molten carbonates. The CO_2 permeation tests at high temperatures were performed, first using a feed gas mixture composed by CO_2/He/N_2 and then with a CO_2/He/O_2/N_2 gas mixture. In both cases, N_2 was used as carrier and sweeping gas. It was observed that the CO_2 separation mechanism, in the latter case was assisted by providing more oxygen species due to the reaction between the feed O_2 and the perovskite electrons which increase the total CO_2 permeation. Prepared membranes exhibit high CO_2/He selectivity values of 40. Furthermore, results suggest that membranes are thermally and chemically stable. Finally, further research must be done on this membrane system in order to elucidate its long-term stability performance as well as to enhance the observed permeation flux. In the later case, both membrane thickness and microstructural control are potential fields of study.

Acknowledgment

O. Ovalle thanks to CONACYT for financial support. J. Ortiz-Landeros thanks to IPN-EDI, IPN-SIBE and SIP-20170426 programs.

Funding

This work was financially supported by the project SENER-CONACYT 251801.

References

[1] H. Pfeiffer, Advances on alkaline ceramics as possible CO_2 captors, in: H. YunHang (Ed.), Adv. CO_2 Convers. Util. ACS Symp. Ser. 1056 American Chemical Society, Washington DC, 2010.
[2] R. Stuart Haszeldine, Carbon capture and storage: how green can black be? Science 325 (80) (2009) 1647–1652.
[3] H.M. Kvamsdal, K. Jordal, O. Bolland, A quantitative comparison of gas turbine cycles with CO_2 capture, Energy 32 (2007) 10–24.
[4] T.C. Merkel, H. Lin, X. Wei, R. Baker, Power plant post-combustion carbon dioxide capture: an opportunity for membranes, J. Membr. Sci. 359 (2010) 126–139.
[5] S. Lee, J.-W. Choi, S.-H. Lee, Separation of greenhouse gases (SF6, CF4 and CO_2) in an industrial flue gas using pilot-scale membrane, Sep. Purif. Technol. 148 (2015) 15–24.
[6] S. Zhao, P.H.M. Feron, L. Deng, E. Favre, E. Chabanon, S. Yan, J. Hou, V. Chen, H. Qi, Status and progress of membrane contactors in post-combustion carbon capture: a state-of-the-art review of new developments, J. Membr. Sci. 511 (2016) 180–206.
[7] D. Jansen, M. Gazzani, G. Manzolini, E. Van Dijk, M. Carbo, Pre-combustion CO_2 capture, Int. J. Greenh. Gas Control 40 (2015) 167–187.
[8] A.S. Damle, T.P. Dorchak, Recovery of carbon dioxide in advanced fossil energy conversion processes using a membrane reactor, J. Energy Environ. Res. 1 (2001) 77–89.
[9] A.L. Karemore, P.D. Vaidya, R. Sinha, On the dry and mixed reforming of methane over Ni/Al_2O_3- Influence of reaction variables on syngas production, Int. J. Hydrog. Energy (2016) 1–13.
[10] M.V. Tsodikov, A.S. Fedotov, D.O. Antonov, V.I. Uvarov, V.Y. Bychkov, F.C. Luck, Hydrogen and syngas production by dry reforming of fermentation products on porous ceramic membrane-catalytic converters, Int. J. Hydrog. Energy 41 (2016) 2424–2431.
[11] S.J. Chung, J.H. Park, D. Li, J.I. Ida, I. Kumakiri, J.Y.S. Lin, Dual-phase metal-carbonate membrane for high-temperature carbon dioxide separation, Ind. Eng. Chem. Res. 44 (2005) 7999–8006.
[12] J.L. Wade, C. Lee, A.C. West, K.S. Lackner, Composite electrolyte membranes for high temperature CO_2 separation, J. Membr. Sci. 369 (2011) 20–29.
[13] L. Zhang, N. Xu, X. Li, S. Wang, K. Huang, W.H. Harris, W.K.S. Chiu, High CO_2 permeation flux enabled by highly interconnected three-dimensional ionic channels in selective CO_2 separation membranes, Energy Environ. Sci. 5 (2012) 8310.
[14] T.T. Norton, J. Ortiz-Landeros, Y.S. Lin, Stability of La-Sr-Co-Fe oxide-carbonate dual-phase membranes for carbon dioxide separation at high temperatures, Ind. Eng. Chem. Res. 53 (2014) 2432–2440.
[15] M. Anderson, Y.S. Lin, Carbonate-ceramic dual-phase membrane for carbon dioxide separation, J. Memb. Sci. 357 (2010) 122–129.
[16] T.T. Norton, Y.S. Lin, Ceramic-carbonate dual-phase membrane with improved chemical stability for carbon dioxide separation at high temperature, Solid State Ion. 263 (2014) 172–179.
[17] Z. Rui, M. Anderson, Y.S. Lin, Y. Li, Modeling and analysis of carbon dioxide permeation through ceramic-carbonate dual-phase membranes, J. Membr. Sci. 345 (2009) 110–118.
[18] X. Zhu, Y. Liu, Y. Cong, W. Yang, $Ce_{0.85}Sm_{0.15}O_{1.9}$25-$Sm_{0.6}Sr_{0.4}Al_{0.3}Fe_{0.7}O_3$ dual-phase membranes: one-pot synthesis and stability in a CO_2 atmosphere, Solid State Ion. 253 (2013) 57–63.
[19] X. Zhu, H. Wang, W. Yang, Relationship between homogeneity and oxygen permeability of composite membranes, J. Membr. Sci. 309 (2008) 120–127.
[20] J. Bergmann, R. Kleeberg, Rietveld Analysis of Disordered Layer Silicates, Mater. Sci. Forum 278–281 (1998) 300–305.
[21] N. Doebelin, R. Kleeberg, Profex: a graphical user interface for the Rietveld refinement program BGMN, J. Appl. Crystallogr. 48 (2015) 1573–1580.
[22] H.P. Klug, L.E. Alexander, X-ray Diffraction Procedures for Polycristalline and Amorphous Materials, 2nd ed., Wiley & Sons, New York, 1974.
[23] J. Ortiz-Landeros, Tyler Norton, Y.S. Lin, Effects of support pore structure on carbon dioxide permeation of ceramic-carbonate dual-phase membranes, Chem. Eng. Sci. 104 (18) (2013) 891–898.
[24] S. Lee, J.H. Yu, S.K. Woo, Dual phase conductive CO_2 membranes: mechanism, microstructure, and electrical conductivity, J. Korean Ceram. Soc. 44 (8) (2007) 424–429.
[25] T.T. Norton, B. Lu, Y.S. Lin, Carbon dioxide permeation properties and stability of samarium-doped-ceria carbonate dual-phase membranes, J. Membr. Sci. 467 (2014) 244–252.
[26] Z. Rui, M. Anderson, Y. Li, Y.S. Lin, Ionic conducting ceramic and carbonate dual phase membranes for carbon dioxide separation, J. Membr. Sci. 417–418 (2012) 174–182.